Earth and Planetary Science Letters, 85 (1987) 145–161
Elsevier Science Publishers B.V., Amsterdam – Printed in The Netherlands

[3]

Dating the lower crust by ion microprobe

Roberta L. Rudnick * and Ian S. Williams

Research School of Earth Sciences, Australian National University, Canberra, A.C.T. 2601 (Australia)

Received February 17, 1987; revised version accepted June 15, 1987

Ion microprobe U-Th-Pb ages of zircons from granulite facies lower crustal xenoliths from north Queensland, Australia, correlate well with the ages of major orogenic episodes manifest at the earth's surface. About half of the xenoliths contain Proterozoic zircons which are similar in age to the episodes of high-grade metamorphism of the older surface rocks. All the xenoliths contain late Paleozoic zircons which show a real 100 Ma range in $^{206}Pb/^{238}U$ ages (from ~ 320 to 220 Ma), which is attributed to granulite facies metamorphism followed by slow cooling in the deep crust. The Paleozoic zircon ages coincide in time with the prolonged episode of eruption of voluminous felsic ash-flows and intrusion of high-level granites in this region (320–270 Ma). Mineral and melt inclusions in the zircons provide clues to the origin of some of the xenoliths, and coupled with the age information, can be used to infer the geological processes operating in the lower crust. The zircons from two mafic xenoliths contain felsic and intermediate melt inclusions implying at least a two-stage history for these rocks, involving either partial melting of a more felsic protolith or crystal accumulation from an evolved melt. Some of the zircons from the felsic xenoliths contain CO_2-rich fluid inclusions, indicating that those zircons grew during high-grade metamorphism. The isotopic and chemical data for the whole rock xenoliths show that they originate from a segment of the lower crust which is a heterogeneous mixture of supracrustal and mafic, mantle-derived, lithologies. The major orogenic event responsible for the formation of that crust occurred in the late Paleozoic, when Proterozoic supracrustal rocks were emplaced into the lower crust, possibly along thin-skinned thrust slices. This was accompanied by intrusion of high-temperature, mantle-derived melts which caused partial melting of pre-existing crust. The most likely setting for such tectonism is a continental margin subduction zone.

1. Introduction

The study of lower crustal xenoliths provides some of the tightest constraints on theories regarding the composition and evolution of the lower crust. The chemical and mineralogical composition of the xenoliths can be used to infer how, but not when, the lower crust formed. Age measurements are crucial to developing crustal growth models, but dating xenoliths is difficult for several reasons. In order to use whole rock Rb-Sr or Sm-Nd methods to determine the age of a suite of xenoliths, the latter must first be shown to be cogenetic. This is rarely possible. Furthermore, if the magma giving rise to a cogenetic suite of xenoliths has variably assimilated country rock, the interpretation of isochrons can be complicated by mixing trends (e.g., [1]). While minerals can provide the metamorphic or cooling ages of xenoliths [2,3], often that age is identical to the age of the host volcanics [4,5], suggesting that xenoliths commonly never cool to, or are reheated above, mineral Rb-Sr and Sm-Nd blocking temperatures prior to eruption. Determining mineral isochrons may not be possible for samples in which texturally complex intergrowths make pure mineral separates difficult to obtain (e.g., Chudleigh province xenoliths [6,7]). Although U-Pb dating of zircon can yield important information on initial crystallization and metamorphic ages of xenoliths [8,9], the mafic compositions of many lower crustal xenoliths [10,11] and their generally small size make obtaining sufficient zircon for conventional U-Pb analyses very difficult. Even single crystal analyses are only averages of the several zircon generations that can be present in any one grain [12]. The U-Pb zircon ages of a suite of lower crustal xenoliths from north Queensland, Australia, have therefore been determined using the

* Present address: Max Planck Inst. für Chemie, Saarstraße 23, Postfach 3060, D 6500 Mainz, F.R.G.

0012-821X/87/$03.50

SHRIMP ion microprobe at the Research School of Earth Sciences, ANU. Use of the ion microprobe overcomes the problems due to small sample size, low zircon content and the presence of multiple zircon populations within each rock.

2. Regional geology

The seven xenoliths investigated here come from a single, late Cenozoic (< 3 Ma) basaltic cinder cone (Hill 32) in the McBride volcanic province of north Queensland (Fig. 1) [13]. The McBride volcanics were erupted onto the eastern edge of the Proterozoic Georgetown Inlier, which is separated from Paleozoic rocks of the Tasman geosyncline by the Palmerville and Burdekin fault zones (Fig. 1). The Palmerville fault zone has recently been interpreted as an imbricate thrust system in which Proterozoic basement rocks were thrust on top of Paleozoic sediments of the Tasman Fold Belt [15]. The last movement on the fault occurred prior to 300 Ma and after ~ 350 Ma [15].

The rock units of the eastern Georgetown Inlier consist of sandstones, carbonates and basalts with minor ultramafics and quartzite. These rocks were folded, metamorphosed to upper amphibolite facies and intruded by granites 1570 ± 20 Ma ago [16]. Some were metamorphosed again at 400 Ma when granites were intruded into the southern margin of the Inlier [16]. The last major orogeny occurred in the late Paleozoic and was accompanied by the eruption of voluminous felsic ash flows and the intrusion of high-level granites (Fig. 1). The ages of these igneous rocks range from 270 to 320 Ma [17]. The very large volumes and unmetamorphosed character of these late Paleozoic rocks suggest that the region has experienced little erosion since this time. Their calc-alkaline composition has led several investigators to postulate their formation in a convergent margin setting [18,19].

3. Samples

Details of the petrography and chemistry of the xenoliths are given in a separate paper [20] and

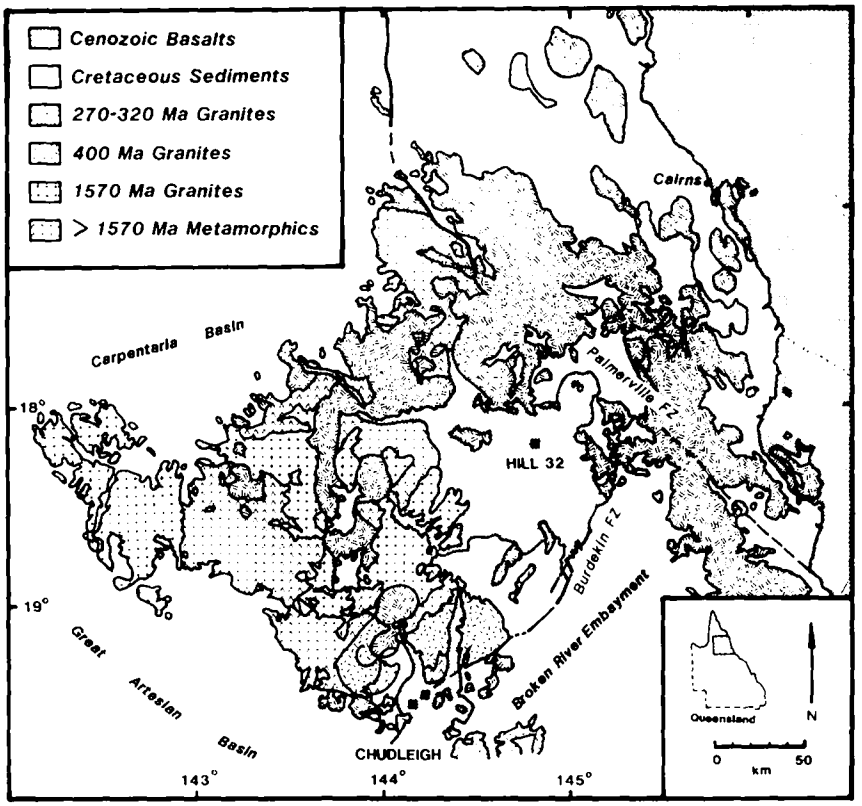

Fig. 1. Generalized geologic map of the eastern Georgetown Inlier area, north Queensland, after [14]. Scale is given in inset.

TABLE 1

Summary of mineralogy and petrogenesis of granulite facies McBride xenoliths

Sample No.	Mineralogy	Zr (ppm)	Equilibration conditions	Petrogenesis
83-162	Q-Kf-Gar-Ap-Zir-Rut-Mt-Il	206	–	felsic meta-igneous rock (adamellite)
83-160	Pc-Q-Opx-Gar-Kf-Cpx-Il-Bio-Mt-Zir	199	750–900 °C [a,b] 1.0–1.1 GPa [c]	felsic meta-igneous rock (granodiorite)
83-157	Pc-Gar-Q-Opx-Bio-Cpx-Rut-Ap-Zir	381	800 °C [d] 0.8–1.0 GPa [c]	metapelite
85-107	Gar-Pc-Q-Cpx-Il-Zir-Ap	1610	680–760 °C [b]	mafic metacumulate
85-100	Opx-Pc-Cpx-Rut-Bio-Il-Ap-Zir	107	960–1000 °C [a]	mafic meta-igneous rock (gabbro)
85-120	Pc-Opx-Cpx-Il-Amph-Rut-Zir	63	860–910 °C [a]	mafic meta-igneous rock (gabbro)
83-159	Pc-Gar-Cpx-Amph-Il-Mt-Rut-Ap-Zir	348	840–920 °C [b]	mafic restite

Minerals are listed in order of decreasing abundance, where Ap = apatite, Amph = amphibole, Bio = biotite, Cpx = clinopyroxene, Gar = garnet, Il = ilmenite, Kf = K-feldspar, Mt = magnetite, Opx = orthopyroxene, Pc = plagioclase, Q = quartz, Rut = rutile, Zir = zircon.

[a] Wells [36]; [b] Ellis and Green [37]; [c] Perkins and Newton [38]; [d] Ferry and Spear [39].

are only summarized here. All xenoliths have high-pressure mineralogies (all are garnet bearing except for the mafic two-pyroxene granulites). The presence of decompression features (i.e., glass along grain boundaries and kelyphitic rims on garnets) suggests these xenoliths are samples of the present-day lower crust rather than near-surface high-grade metamorphic rocks from the Georgetown Inlier. The mineralogy of, and preferred petrogenetic model for each xenolith, as determined from its chemical composition, are listed in Table 1. Whole rock Zr concentrations, indicative of the relative amounts of zircon in each sample, are also listed. The xenoliths range from felsic to mafic meta-igneous rocks and include possible restite material and a metasediment. All have granulite facies mineralogies.

4. Analytical techniques and data reduction methods

All samples were coarsely crushed in a steel jaw crusher and screened, and material less than 200 μm was discarded in order to eliminate possible inter-sample cross-contamination. The remaining sample was then finely crushed in a tungsten carbide swing mill. The powder was washed in water to remove the fines, then the zircons were concentrated using standard heavy liquid and magnetic separation techniques. The final split was handpicked and the zircons mounted in epoxy and polished to expose their centers.

U-Th-Pb measurements were made on 20–30 μm diameter regions of single zircons using the SHRIMP ion microprobe [21,22]. SHRIMP was operated at a mass resolution of about 6500 in order to eliminate all significant isobaric interferences. Pb isotopic compositions were determined directly, with no correction for the small amount of mass dependent mass fractionation (2.5‰ per mass unit) that may occur during sputtering and ion extraction [22]. Pb/U ratios were determined relative to a reference Sr Lankan zircon (SL3) using an empirical quadratic relationship between Pb^+/U^+ and UO^+/U^+ established from multiple analyses of this standard.

Corrections for common Pb were made either from the measured $^{204}Pb/^{206}Pb$ (designated with superscript "a" in Table 2) or $^{208}Pb/^{206}Pb$ and Th/U (designated with superscript "b" in Table 2). The latter method was preferred because of its higher precision, but the former was used in cases where changes in $^{208}Pb/^{206}Pb$ or Th/U were known or suspected to have occurred other than by radioactive decay.

Analytical uncertainties in the determination of the Pb isotopic compositions were dominated by counting statistics. The uncertainties in Pb/U were dominated by uncertainty in the quadratic calibration curve for each analytical session; on average Pb/U was determined to a precision of about 2% (1σ) per data set. The precise value of this uncertainty was calculated from analyses of the standard for each analytical session and added to the

TABLE 2

Representative isotopic analyses of zircons from granulite facies McBride Province xenoliths

Grain spot	$^{207}Pb^*/^{206}Pb^*$ ±1σ	$^{206}Pb^*/^{238}U$ ±1σ	$^{207}Pb^*/^{235}U$ ±1σ	$^{208}Pb^*/^{232}Th$ ±1σ	Conc. (ppm) U	Th	Pb*	Th/U	f (%)	Apparent age (Ma) 206/238 ±1σ	207/206 ±1σ
83-162 [b]											
4-1	0.0567 ± 54	0.0583 ± 12	0.456 ± 45	-	102	109	7	1.076	-	365 ± 7	480 ± 200
4-1′	0.0533 ± 64	0.0484 ± 10	0.356 ± 45	-	104	105	6	1.007	5.4	305 ± 5	350 ± 200
4-2C	0.0431 ± 61	0.0451 ± 9	0.268 ± 39	-	91	93	5	1.023	1.4	284 ± 6	5 ± 105
4-3	0.0460 ± 83	0.0441 ± 9	0.280 ± 52	-	128	141	7	1.100	6.9	278 ± 6	40 ± 300
11-1C	0.0553 ± 34	0.0313 ± 12	0.238 ± 18	-	641	660	24	1.029	3.3	198 ± 8	430 ± 130
11-2	0.0501 ± 25	0.0344 ± 13	0.238 ± 16	-	761	586	29	0.769	1.6	218 ± 8	200 ± 110
13-1C	0.0499 ± 27	0.0360 ± 7	0.248 ± 15	-	325	286	13	0.881	1.5	228 ± 5	200 ± 120
13-2R	0.0531 ± 23	0.0382 ± 8	0.280 ± 14	-	304	37	11	0.123	1.2	242 ± 4	340 ± 90
14-1C	0.0466 ± 31	0.0376 ± 8	0.242 ± 17	-	237	170	10	0.716	2.5	238 ± 5	60 ± 120
14-2R	0.0478 ± 20	0.0357 ± 7	0.235 ± 12	-	374	147	13	0.392	1.3	226 ± 5	100 ± 90
16-1C	0.0516 ± 35	0.0437 ± 9	0.310 ± 23	-	137	80	6	0.583	1.6	276 ± 5	270 ± 150
16-2R	0.0518 ± 14	0.0358 ± 7	0.255 ± 9	-	616	35	20	0.057	0.7	226 ± 5	280 ± 60
18-1 [a]	0.0487 ± 160	0.0410 ± 11	0.275 ± 91	0.0134 ± 6	59	372	6	6.350	5.4	259 ± 7	140 ± 600
19-1	0.0496 ± 28	0.0402 ± 8	0.275 ± 17	-	328	355	16	1.083	1.1	254 ± 5	180 ± 130
20-1 [a]	0.0363 ± 130	0.0364 ± 9	0.182 ± 66	0.0120 ± 5	116	490	8	4.224	5.4	231 ± 6	2 ± 120
21-1	0.0565 ± 46	0.0377 ± 8	0.293 ± 25	-	167	155	7	0.930	1.8	238 ± 5	470 ± 170
22-1	0.0523 ± 50	0.0370 ± 8	0.267 ± 27	-	184	257	9	1.395	2.5	234 ± 5	300 ± 200
23-1	0.0531 ± 16	0.0355 ± 7	0.260 ± 10	-	904	715	36	0.791	0.5	225 ± 4	340 ± 65
24-1	0.0285 ± 408	0.0371 ± 19	0.14 ± 21	-	105	495	8	4.704	7.6	235 ± 12	-
83-160 [b]											
1-1	0.0564 ± 11	0.0392 ± 8	0.305 ± 9	-	1654	457	64	0.276	1.4	248 ± 4	470 ± 40
1-1′	0.0535 ± 24	0.0298 ± 18	0.219 ± 17	-	580	370	19	0.638	2.2	189 ± 11	350 ± 100
2-1	0.0500 ± 23	0.0423 ± 8	0.291 ± 15	-	695	427	31	0.615	4.5	267 ± 5	195 ± 100
5-1	0.0553 ± 46	0.0365 ± 7	0.278 ± 24	-	386	262	15	0.679	7.7	231 ± 5	420 ± 170
7-1	0.0540 ± 30	0.0567 ± 11	0.422 ± 26	-	404	141	23	0.349	6.9	355 ± 7	375 ± 125
8-1	0.0585 ± 61	0.0312 ± 6	0.252 ± 28	-	391	472	15	1.207	10.3	198 ± 4	550 ± 250
8-1′	0.0494 ± 47	0.0304 ± 18	0.207 ± 25	-	292	364	11	1.246	3.2	193 ± 11	170 ± 200
12-1 [a]	0.1387 ± 22	0.3972 ± 81	7.59 ± 21	0.1108 ± 37	436	266	195	0.612	1.4	2156 ± 140	2211 ± 25
12-2 [a]	0.1389 ± 16	0.329 ± 20	6.30 ± 39	0.0905 ± 57	356	234	133	0.656	1.1	1834 ± 96	2214 ± 21
14-1	0.0623 ± 100	0.0330 ± 20	0.283 ± 51	-	139	236	6	1.691	9.2	209 ± 13	680 ± 310
15-1	0.05257 ± 20	0.0358 ± 22	0.260 ± 19	-	590	351	23	0.596	0.6	227 ± 13	315 ± 80
16-1	0.0525 ± 40	0.0392 ± 24	0.283 ± 29	-	157	104	7	0.664	2.8	248 ± 14	310 ± 160
85-107 round [b]											
1-1	0.0547 ± 28	0.0448 ± 7	0.338 ± 19	-	169	36	7	0.211	2.15	283 ± 5	400 ± 110
11-1C	0.0540 ± 23	0.0509 ± 8	0.378 ± 18	-	351	289	20	0.824	1.44	320 ± 5	370 ± 90
17-1	0.0529 ± 16	0.0384 ± 6	0.280 ± 10	-	483	32	17	0.066	1.51	243 ± 4	330 ± 65
85-107 elongate [b]											
2-2AC	0.0600 ± 55	0.0494 ± 8	0.407 ± 39	-	156	39	7	0.250	4.79	311 ± 5	600 ± 190
4-1	0.0566 ± 18	0.0535 ± 9	0.417 ± 15	-	499	312	29	0.625	0.96	336 ± 5	476 ± 67
5-1C	0.0545 ± 13	0.402 ± 7	0.302 ± 9	-	831	311	34	0.374	0.70	254 ± 4	393 ± 53
5-2	0.0527 ± 15	0.0382 ± 6	0.278 ± 10	-	735	399	30	0.543	0.58	242 ± 4	321 ± 60
8-1	0.0729 ± 81	0.0470 ± 8	0.472 ± 54	-	59	35	3	0.600	7.57	296 ± 5	1010 ± 210
13-1	0.00453 ± 59	0.0380 ± 6	0.237 ± 31	-	99	39	4	0.398	5.06	241 ± 4	30 ± 220
14-1	0.0665 ± 68	0.0418 ± 7	0.383 ± 40	-	77	34	3	0.440	7.58	264 ± 4	820 ± 200
83-157 round [b]											
1-1	0.0616 ± 44	0.0389 ± 8	0.331 ± 25	-	231	58	9	0.251	10.9	246 ± 5	660 ± 150
5-2	0.0599 ± 119	0.0368 ± 8	0.304 ± 61	-	131	85	5	0.651	23.2	233 ± 5	600 ± 380
13-1	0.0806 ± 310	0.0396 ± 14	0.44 ± 17	-	74	141	4	1.901	38.3	250 ± 9	1210 ± 680

TABLE 2 (continued)

Grain spot	$^{207}Pb^*/^{206}Pb^*$ ±1σ	$^{206}Pb^*/^{238}U$ ±1σ	$^{207}Pb^*/^{235}U$ ±1σ	$^{208}Pb^*/^{232}Th$ ±1σ	Conc. (ppm) U	Th	Pb*	Th/U	f (%)	Apparent age (Ma) 206/238 ±1σ	207/206 ±1σ
83-157 elongate [a]											
2-1C	0.1272 ± 15	0.3856 ± 78	6.76 ± 17	0.1466 ± 76	396	65	156	0.165	0.59	2100 ± 35	2060 ± 20
2-2	0.1200 ± 69	0.1866 ± 40	3.09 ± 20	0.0511 ± 80	164	58	32	0.357	2.62	1100 ± 20	1960 ± 100
2-3 [b]	0.0975 ± 13	0.2570 ± 52	3.45 ± 9	-	444	65	112	0.147	3.59	1474 ± 31	1576 ± 24
3-1C	0.0967 ± 10	0.2028 ± 41	2.70 ± 6	0.0534 ± 24	1066	191	213	0.179	0.48	1190 ± 22	1562 ± 18
3-2	0.1020 ± 13	0.3117 ± 63	4.38 ± 11	0.0971 ± 58	602	91	185	0.151	0.70	1749 ± 31	1661 ± 24
3-3	0.0842 ± 60	0.1397 ± 29	1.62 ± 12	0.0327 ± 72	265	69	36	0.260	3.34	843 ± 17	1300 ± 130
7-1C	0.0932 ± 42	0.2427 ± 51	3.12 ± 16	0.0691 ± 51	265	126	68	0.472	2.23	1401 ± 26	1491 ± 84
7-2	0.0986 ± 25	0.3370 ± 69	4.59 ± 16	0.0983 ± 52	341	134	120	0.391	1.29	1876 ± 34	1598 ± 50
7-3	0.0958 ± 30	0.3411 ± 70	4.5 ± 18	0.0916 ± 57	366	154	130	0.420	1.61	1892 ± 33	1545 ± 60
12-2	0.0997 ± 66	0.2076 ± 45	2.85 ± 20	0.0690 ± 89	204	72	44	0.350	3.36	1216 ± 23	1620 ± 110
16-1	0.0904 ± 44	0.2772 ± 58	3.45 ± 19	0.0779 ± 66	375	162	108	0.432	2.69	1577 ± 28	1435 ± 90
16-2C [b]	0.965 ± 13	0.2726 ± 55	3.63 ± 9	-	507	257	147	0.507	1.82	1554 ± 28	1558 ± 23
16-3	0.0968 ± 28	0.3188 ± 66	4.25 ± 16	0.0967 ± 48	439	202	149	0.459	0.85	1784 ± 33	1562 ± 55
20-1	0.0984 ± 23	0.2627 ± 53	3.56 ± 12	0.0755 ± 37	286	112	78	0.391	0.26	1504 ± 91	1595 ± 42
20-2	0.0967 ± 16	0.2948 ± 60	3.93 ± 11	0.0891 ± 28	234	109	73	0.467	0.32	1666 ± 30	1562 ± 30
23-1C	0.0990 ± 17	0.1810 ± 36	2.47 ± 7	0.0420 ± 22	569	93	103	0.173	0.03	1073 ± 20	1605 ± 32
85-100 [b]											
1-1	0.0537 ± 50	0.0617 ± 13	0.456 ± 45	-	83	90	6	1.081	5.07	386 ± 8	360 ± 200
1-2	0.0745 ± 84	0.0454 ± 10	0.466 ± 54	-	74	87	4	1.174	10.4	286 ± 6	1050 ± 210
2-1	0.0655 ± 42	0.0531 ± 11	0.480 ± 33	-	160	188	11	1.174	2.13	333 ± 7	790 ± 130
3-1	0.0571 ± 16	0.0547 ± 11	0.430 ± 15	-	480	52	25	0.108	2.42	343 ± 7	495 ± 60
5-1	0.0743 ± 63	0.097 ± 8	0.406 ± 36	-	133	206	7	1.552	3.18	251 ± 5	1050 ± 160
6-1	0.0607 ± 27	0.0586 ± 12	0.491 ± 25	-	300	109	18	0.363	5.28	367 ± 8	630 ± 90
10-1C	0.0679 ± 14	0.1280 ± 26	1.199 ± 37	-	452	221	61	0.489	2.56	777 ± 15	867 ± 43
10-2	0.0579 ± 19	0.0594 ± 12	0.474 ± 19	-	405	19	22	0.046	2.73	372 ± 7	526 ± 68
11-1	0.0818 ± 17	0.1935 ± 39	2.183 ± 67	-	250	208	55	0.829	0.92	1140 ± 22	1241 ± 41
12-1	0.0765 ± 17	0.1733 ± 35	1.829 ± 58	-	246	126	45	0.513	1.86	1030 ± 20	1109 ± 44
85-120 [b]											
1-1	0.0486 ± 77	0.0439 ± 9	0.294 ± 48	-	103	23	4	0.223	11.0	277 ± 6	130 ± 330
1-2	0.0660 ± 57	0.0416 ± 15	0.378 ± 37	-	70	13	3	0.192	4.24	263 ± 9	810 ± 170
3-2	0.0599 ± 144	0.0382 ± 14	0.316 ± 63	-	29	6	1	0.199	11.4	243 ± 8	600 ± 370
4-1	0.0508 ± 36	0.0545 ± 12	0.382 ± 66	-	80	82	5	1.024	8.58	342 ± 7	230 ± 350
4-2	0.0622 ± 65	0.0477 ± 17	0.410 ± 47	-	69	68	4	0.982	3.91	301 ± 10	680 ± 210
6-1	0.0527 ± 9	0.0411 ± 8	0.299 ± 8	-	1448	217	56	0.150	0.72	260 ± 5	320 ± 30
6-2	0.0607 ± 71	0.0340 ± 12	0.284 ± 36	-	68	46	3	0.680	5.98	215 ± 8	630 ± 230
8-1	0.0528 ± 73	0.0348 ± 7	0.253 ± 36	-	152	135	17	0.889	5.74	220 ± 4	330 ± 280
8-2	0.0518 ± 45	0.0338 ± 12	0.241 ± 24	-	162	153	6	0.946	3.32	214 ± 7	280 ± 190
16-1	0.0669 ± 127	0.0403 ± 15	0.372 ± 73	-	22	6	1	0.266	9.28	255 ± 8	840 ± 350
83-159 [b]											
1-1	0.0578 ± 24	0.0381 ± 4	0.304 ± 13	-	279	49	10	0.176	2.77	241 ± 3	520 ± 90
1-2	0.0560 ± 22	0.0355 ± 7	0.274 ± 13	-	355	48	12	0.136	1.25	225 ± 4	450 ± 80
3-1′ [a]	0.0860 ± 30	0.1312 ± 27	1.555 ± 66	0.0344 ± 33	154	40	20	0.261	1.40	795 ± 15	1340 ± 70
3-2	0.0639 ± 34	0.0765 ± 8	0.674 ± 38	-	173	99	14	0.572	4.54	475 ±	740 ±
3-3§ [a]	0.0710 ± 26	0.0669 ± 7	0.655 ± 26	0.0243 ± 7	228	126	16	0.555	0.11	418 ± 4	960 ± 75
3-4 [a]	0.0767 ± 46	0.0999 ± 21	1.057 ± 70	0.0228 ± 38	163	45	16	0.279	2.83	614 ± 12	1110 ± 115
6-1	0.0456 ± 32	0.0376 ± 4	0.236 ± 17	-	224	69	8	0.311	3.35	238 ± 2	30 ± 110
6-2 [a]	0.0860 ± 26	0.1078 ± 22	1.278 ± 50	0.0819 ± 55	187	62	20	0.333	0.94	660 ± 13	1340 ± 60
13-1	0.0949 ± 18	0.1265 ± 13	1.655 ± 38	-	244	66	31	0.272	0.36	768 ± 7	1526 ± 34
13-2	0.0545 ± 28	0.0523 ± 11	0.394 ± 23	-	211	94	11	0.445	2.47	329 ± 6	395 ± 110
23-1C [a]	0.0939 ± 36	0.2797 ± 58	3.620 ± 165	0.085 ± 12	344	62	95	0.180	1.36	1590 ± 30	1510 ± 70
23-2	0.0789 ± 35	0.0641 ± 13	0.697 ± 35	-	317	60	20	0.190	4.04	400 ± 8	1170 ± 85
23-3 [a]	0.0909 ± 13	0.1873 ± 47	2.347 ± 72	0.0315 ± 25	236	44	43	0.188	0.69	1107 ± 26	1445 ± 27
27-1§	0.0556 ± 65	0.0326 ± 7	0.250 ± 30	-	234	34	7	0.146	7.96	207 ± 4	440 ± 240

TABLE 2 (continued)

Grain spot	$^{207}Pb^*/^{206}Pb^*$ ±1σ	$^{206}Pb^*/^{238}U$ ±1σ	$^{207}Pb^*/^{235}U$ ±1σ	$^{208}Pb^*/^{232}Th$ ±1σ	Conc. (ppm) U	Th	Pb*	Th/U	f (%)	Apparent age (Ma) 206/238 ±1σ	207/206 ±1σ
28-1§	0.0508 ±126	0.0275 ± 6	0.193 ± 48	–	167	36	4	0.213	19.3	175 ± 4	320 ± 490
29-1 [a]	0.0865 ± 55	0.2576 ± 56	3.073 ± 214	0.021 ±20	268	41	65	0.153	1.93	1478 ± 37	1350 ± 120
29-4 [a]	0.0924 ± 12	0.2068 ± 52	2.634 ± 79	0.0482 ± 23	238	54	48	0.225	0.41	1211 ± 28	1476 ± 24
30-1 [a]	0.0859 ±120	0.0936 ± 22	1.109 ± 160	0.0302 ± 87	260	77	25	0.294	2.77	577 ± 13	1340 ± 250
31-1	0.0512 ± 18	0.0377 ± 9	0.266 ± 12	-	282	31	10	0.110	1.05	238 ± 6	250 ± 80
32-1	0.05910 ± 43	0.0329 ± 8	0.268 ± 22	-	105	54	4	0.515	3.37	208 ± 5	570 ± 150

* Radiogenic Pb; [a] Common Pb corrected using ^{204}Pb; [b] Common Pb corrected using ^{208}Pb.
f (%) denotes percent of common ^{206}Pb in the total measured ^{206}Pb.
Spot numbers in italics are analyses corrected for high background, as described in Appendix 1.
An ′ after spot number indicates a duplicate analysis on same spot.
C after spot number means spot was in core of crystal.

counting and common Pb correction uncertainties in the analysis of each sample. Unless stated otherwise, uncertainties in the ages quoted in this paper are 95% confidence limits. Regression analyses were made using the coordinate system $^{207}Pb/^{206}Pb$-$^{238}U/^{206}Pb$ to minimize the effects of correlated errors [23], and the 95% confidence limits for intercept ages so determined are given as t sigma. The decay constants used here are those recommended by the IUGS Subcommission on Geochronology [24].

The zircon analyses were made over a 10 month period. About one third of this work was done soon after modifications to SHRIMP's ion counting system (to permit multiple collection of titanium isotopes) and corrections for scattered ions, at times as high as 15 counts/second, were required. The remaining analyses were made after the problem of scattering had been overcome, and included a large number of duplicate runs on areas studied previously. Through a comparison of the duplicates it was determined that the first correction for scattered ions, which had assumed a constant flux of scattered ions independent of the mass analyzed, had been incorrect. The flux of scattered ions at mass 207 was in fact higher than at mass 206, in direct proportion to the 196 (Zr_2O) count rate, leading to a consistent overestimation of the $^{207}Pb/^{206}Pb$ ratio. The effect of the overestimation was most serious for zircons with low radiogenic ^{207}Pb contents (young, low-U zircons), but could be corrected out by a simple procedure outlined in Appendix A. Data so corrected are shown in italics in Table 2.

Chemical compositions of mineral and melt inclusions in the zircons were measured using a wavelength dispersive Cameca electron probe. Mineral inclusions were analyzed using a 15 nA beam current and focused beam; melt inclusions were analyzed with a 10 nA beam current and rastered beam in order to minimize alkali volatilization. Because zircon fluoresces strongly under electron bombardment, it was possible to determine precisely when the beam was hitting the inclusion, even when they were extremely small.

Fluid inclusions were identified either by the presence of a moving vapor bubble, or, more commonly, by the nucleation of a vapor bubble within single phase inclusions upon cooling with Freon. Their composition was estimated by observations on homogenization and freezing behavior. All two-phase inclusions homogenized to a fluid at temperatures below 30 °C and did not crystallize upon cooling to temperatures of −30 °C. These observations, plus the absence of daughter phases suggests that the fluid inclusions are CO_2-rich. However, because melting experiments have not been performed, the relative purity of the CO_2 has not been determined.

5. Zircon characteristics and U-Pb results

Representative zircon U-Th-Pb analyses are listed in Table 2. Due to space limitations only half of the full data set is presented, a complete set of analyses is available from the Research School of Earth Sciences upon request. The zircon morphologies and the types of inclusions they

contain are clues to the igneous and metamorphic histories of their immediate host rocks and help in interpreting the isotopic ages. None of the zircons are optically zoned or strongly colored, probably because of the annealing of their structures during the granulite facies metamorphism and subsequent residence in a warm, lower crustal environment. The zircons from several samples show cleavage

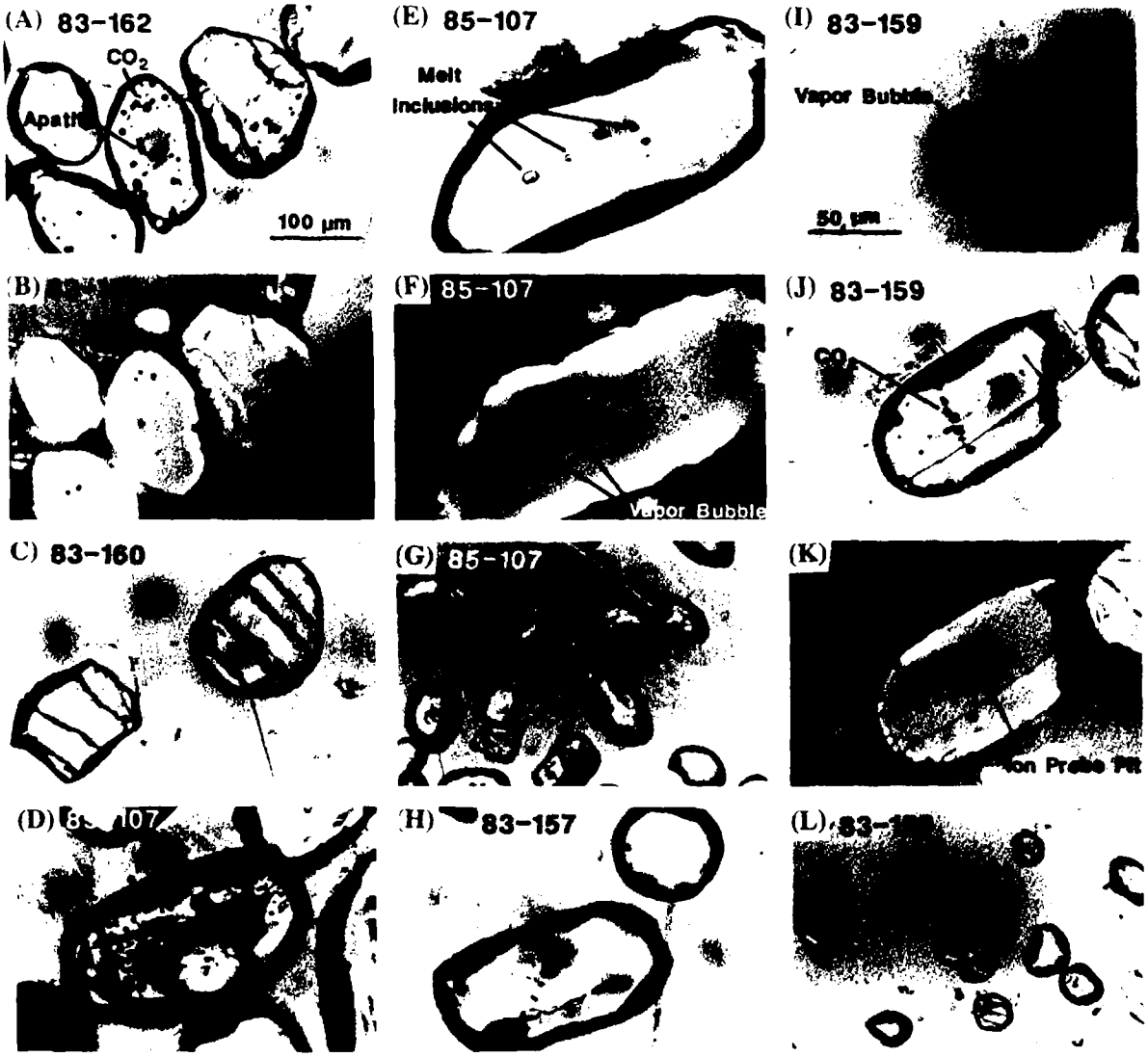

Fig. 2. Zircon features. Scale for all photos, except (I) is given by scale bar at lower right corner of photo (A). (A) Transmitted light photo of zircons from 83-162 containing CO_2-rich fluid inclusions near the outer regions of the grain (dark spots). (B) Same as (A) only in reflected light. Note that inclusions are empty when they intersect the surface (as seen by their low reflectivity). (C) Zircons from 83-160 showing parallel partings (transmitted light). (D) Zircon from 85-107 which contains small, round melt inclusions in center (E) Relatively large melt inclusions in elongate zircon (#19), which were analyzed by electron probe (Table 3). Immobile vapor bubble is visible in two inclusions on left (transmitted light). (F) Same zircon as in (E) in reflected light, note that vapor bubble within melt inclusion is empty. Large depression near center of zircon is ion probe spot. (G) Pinched zircon in 85-107. (H) Morphological varieties of zircons from 83-157: round and elongate. (I) Reflected light photo of a crystallized melt inclusion in zircon from 83-159: empty, distorted vapor bubble at upper left, euhedral amphibole crystals at lower right and bright, euhedral sulfide crystal at upper right. Reintegrated composition of this inclusion is given in Table 3. (J) Trail of CO_2-rich fluid inclusions cross-cutting zircon in 83-159. (I) Same as (J) only in reflected light. (L) Parallel partings in zircons from 83-159.

traces or partings which may be a response to rapid decompression during eruption. Similar partings have been noted in some kimberlite zircons by Kresten et al. [25].

5.1. 83-162 meta-adamellite

The zircons in adamellite xenolith 83-162 are clear, colorless and generally rounded, although some are elongate. About half of them contain CO_2-rich fluid inclusions (Fig. 2A, B), which define a concentric shell within the crystals, suggesting they were trapped at a late stage of zircon growth. CO_2-rich fluid inclusions are ubiquitous in a variety of minerals from high-pressure granulites [26,27] thus suggesting that at least the rims of these zircons grew during granulite facies metamorphism. Quartz, K-feldspar and rutile inclusions occur in some zircons, and apatite has been observed in the core of a few zircons.

These zircons have a wide range of Th/U, from

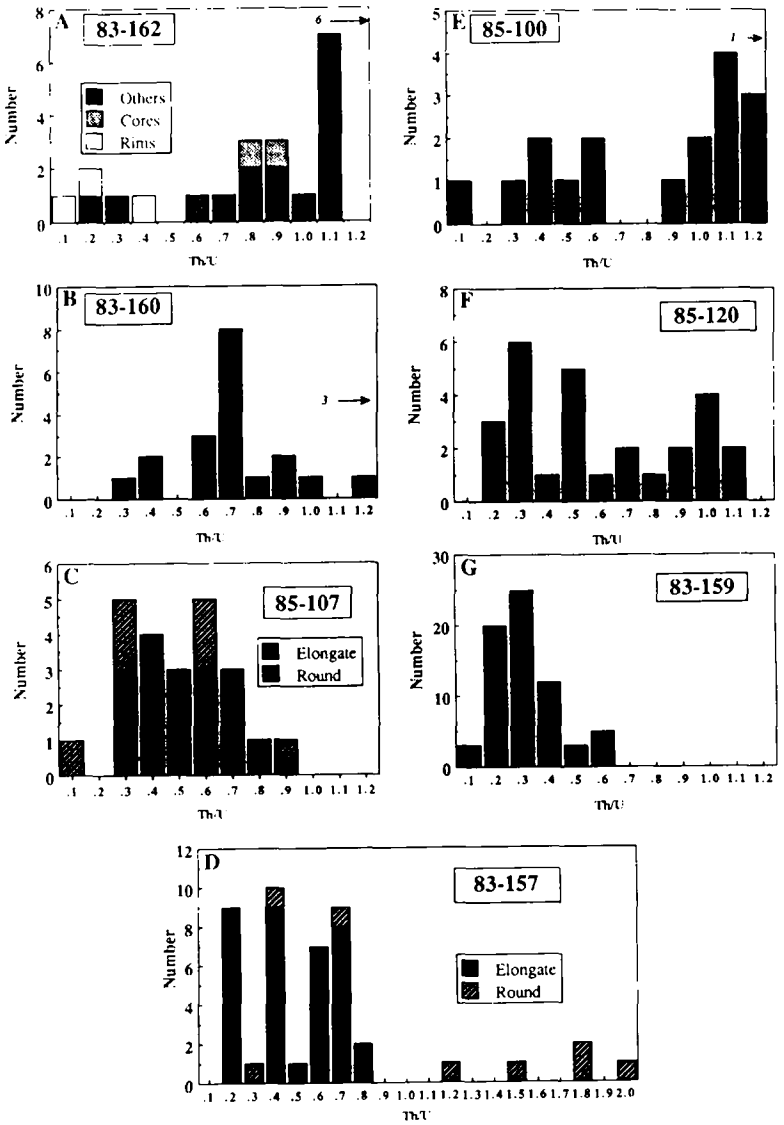

Fig. 3. Histograms of Th/U ratios in zircons. (A) 83-162, cores and rims are defined by the location of CO_2-rich fluid inclusions (see Fig. 2A). Note peak near Th/U = 1. (B) 83-160. (C) 85-107, with two morphological types of zircons distinguished. (D) 83-157, with two morphological types of zircons distinguished. (E) 85-100. (F) 85-120. (G) 83-159, note low average Th/U ratio for this sample.

0.06 to 6.4, but most are near 1.0 (Fig. 3A); thus zircons from this sample have the highest average Th/U of the suite. Zircons from granites (sensu lato) generally have Th/U between 0.1 and 1.0, with an average of 0.5 and a mode of 0.3 (from 72 analyses [28]). Although it could be argued that the very high Th/U ratios in the zircons from 83-162 reflect U depletion due to metamorphism, this is not supported by the fact that Th/U of the rims of the fluid inclusion-bearing zircons is distinctly lower than in their cores (Fig. 3A). There is also a considerable range in Th and U concentrations (Table 2), but no correlation between Th and U concentrations and Th/U.

The $^{206}Pb/^{238}U$ ages range from 200 to 370 Ma, with nearly all zircons plotting within error of concordia (Fig. 4A). In these, and the other Paleozoic zircons from the other xenoliths, the $^{206}Pb/^{238}U$ age is a much more precise, and probably a more accurate, indicator of closure age than

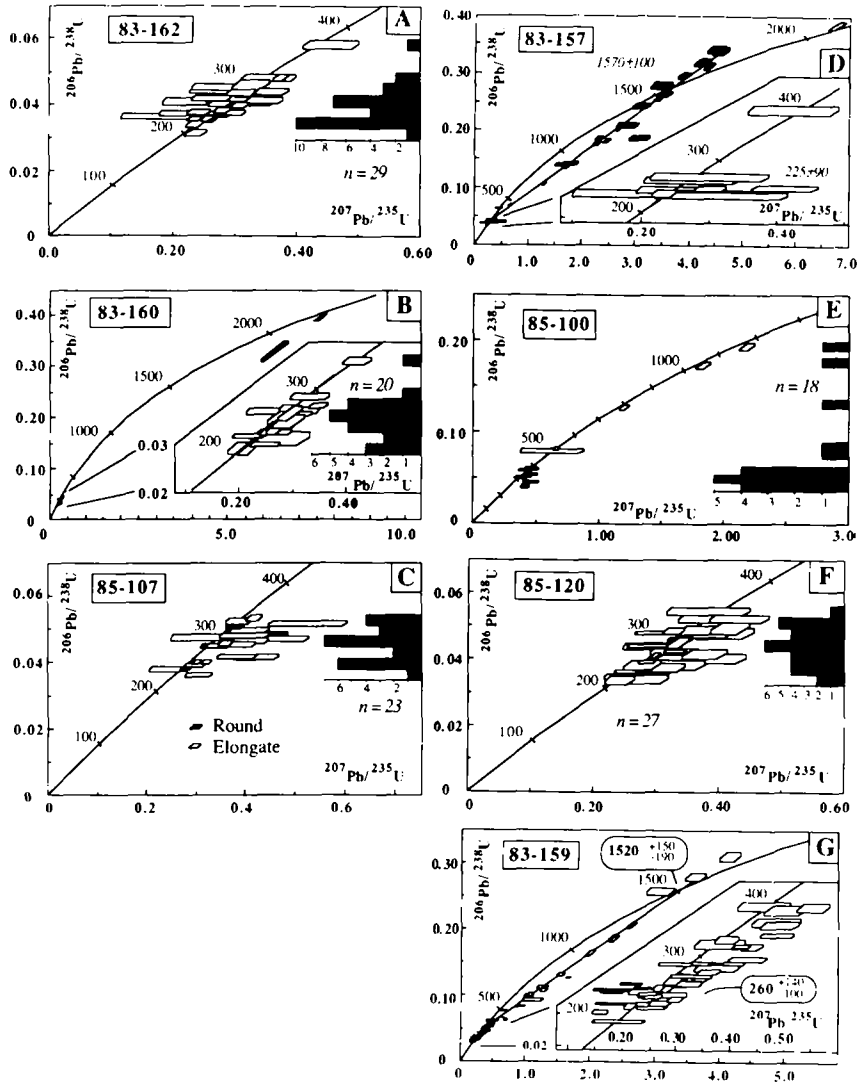

Fig. 4. (A–G) Concordia plots for lower crustal xenoliths, with sample numbers given on each figure. Error boxes represent 1σ mean. Histograms at right show distribution of $^{206}Pb/^{238}U$ ages, with interval set equal to approximately 2σ uncertainty (i.e., 20 Ma). Insets for 83-160, 83-157 and 83-159 show detail at lower ends of concordia. The solid boxes in (B) are separate analyses for a single old zircon. The shaded boxes in (D) are separate analyses of one old zircon; solid boxes are elongate zircons and open boxes are rounded zircons.

the $^{207}Pb/^{206}Pb$ age. This is because the measurements of the extremely small amounts of radiogenic ^{207}Pb in the young, low-U zircons are subject to large uncertainties due to counting statistics and uncertainties in common Pb correction. Radiogenic ^{206}Pb, being a factor of 20 times more abundant, is much more precisely determined. For this reason, histograms of $^{206}Pb/^{238}U$ ages are plotted on the concordia diagrams in Fig. 4.

There is no correlation between the age and Th and U content or Th/U for the zircons in 83-162. The cores and rims of three zircons containing CO_2 rich fluid inclusions either have indistinguishable ages (grains 13 and 14) or slightly older cores (grain 16). The zircon with the highest measured $^{206}Pb/^{238}U$ age (#4, 365 ± 7 Ma) is elongate, rather than round, and lacks CO_2-rich fluid inclusions. The zircon with the youngest $^{206}Pb/^{238}U$ age (#11, 198 ± 8 Ma) is necked, and contains abundant CO_2-rich fluid inclusions. It is likely that the zircon's isotopic compositions predominantly reflect high-grade metamorphism in the late Paleozoic-early Mesozoic. The significant range in $^{206}Pb/^{238}U$ ages in the cluster between ~ 300 and ~ 200 Ma may result from the varied response of ≥ 300 Ma zircons to a ~ 230 Ma metamorphism or from slow cooling after an earlier peak metamorphism. Is is not possible to date the crystallization age of the original adamellite melt precisely; it could be ≥ 365 Ma (from grain 4), or it may be ~ 300 Ma, if grain 4 is a xenocryst.

5.2. *83-160 metagranodiorite*

Granodioritic xenolith 83-160 contains clear, strongly rounded zircons, which commonly have parallel cleavage traces or partings (Fig. 2C). CO_2-rich fluid inclusions occur near the outer rims in many of the grains, although they are not as abundant as in zircons from 83-162. Elongate apatite and cubic Fe-sulfide inclusions also occur.

Th and U concentrations vary by an order of magnitude, but Th/U ratios cluster around 0.7 ($\sigma = 0.26$) (Fig. 3B, Table 2). There is no correlation between Th and U concentrations and Th/U.

All zircons but one have $^{206}Pb/^{238}U$ ages between 190 and 350 Ma and nearly all lie on concordia (Fig. 4B). The exception (grain 12), which may be an inherited crystal, is ~ 2200 Ma old. Within the young zircons there is a rough negative correlation between $^{206}Pb/^{238}U$ ages and Th/U, suggesting that as the zircons lost Pb during metamorphism their Th/U increased. The isotopic data suggest the same history for this sample as for meta-adamellite 83-162, except that the oldest xenocryst is ~ 2200 Ma rather than ~ 360 Ma old.

5.3. *85-107 mafic cumulate*

Mafic xenolith 85-107 contains abundant zircon (this sample has 1600 ppm Zr, Table 1) and probably formed as a cumulate from a felsic melt [20]. Zircons in this sample fall into two morphological groups: (1) round, clear zircons and (2) large, elongate, inclusion-rich light brown zircons. The elongate zircons are far more abundant than the round zircons and, in some cases, the elongate zircons are necked in the middle, suggesting breakdown to form the rounded type (Fig. 2G). Many of the elongate zircons are riddled with small (generally < 6 μm) oval inclusions with immobile vapor bubbles at their edges (Fig. 2D, E, F). When they intersect the surface, the vapor bubble is empty and the surrounding material appears homogeneous in reflected light. Electron probe analyses were obtained on some of the larger of these inclusions (> 10 μm) and are listed in Table 3. The inclusions are relatively homogeneous and have the composition of a felsic melt. This homogeneity is consistent with the absence of visible daughter crystals, and suggests these inclu-

TABLE 3

Electron probe analyses of mineral and melt inclusions within zircons.

	85-107 Z7 melt	83-159 Z19 melt [a]	83-159 Z19 amphibole [b]
SiO_2	71.43	63.4	39.5
TiO_2	0.10	0.6	2.9
Al_2O_3	13.05	19.6	16.5
FeO	1.36	2.1	11.3
MgO	0.26	2.3	12.4
CaO	2.41	6.2	11.0
Na_2O	3.18	2.6	3.0
K_2O	3.97	1.2	0.6
Total	95.76	98.0	97.2

[a] Melt inclusion in 83-159 represents estimate based upon integration of matrix and daughter crystal analyses, with relative proportions estimated optically.

[b] Occurs in melt inclusion.

sions represent relatively unmodified trapped melts. Acicular apatite, clinopyroxene, magnetite, ilmenite and pyrrhotite also occur within these zircons. Several features of the inclusions within zircons, i.e., acicular apatite [29] and the absence of daughter crystals in the melt inclusions, are indicative of rapid cooling [27, Ch. 16].

Th and U concentrations in the zircons vary by an order of magnitude (Table 2) and do not correlate with zircon morphology. Th/U ratios are all less than 1.0 (Fig. 3C); Th/U in the round zircons is highly variable but in the elongate zircons is more constant at about 0.46 (± 0.15, 1 σ).

All the zircon analyses fall within error of concordia and have $^{206}Pb/^{238}U$ ages between 240 and 340 Ma (Fig. 4C). The ages do not correlate with crystal morphology or Th/U. The lack of an age difference between the two zircon types, plus the textural evidence of zircon breakdown (i.e., pinched grains) suggests that the round zircons may have formed simply by breakdown of the elongate grains, rather than as a second zircon generation. The range of $^{206}Pb/^{238}U$ ages can thus be attributed to Pb loss rather than recrystallization or new zircon growth.

The presence of felsic melt inclusions within the zircons requires a multistage history for this mafic xenolith. The abundance of zircons suggests they are not xenocrystic. It is more likely that either the zircons crystallized from a felsic melt and accumulated during fractional crystallization of that melt or that they were left behind in the mafic residue after partial melting of an original felsic rock. The relatively short time interval between original igneous crystallization (340 Ma) and metamorphism (not later than 240 Ma ago) would favor a cumulate origin for this rock. The rapid cooling features in the zircon inclusions may have been produced in the deep crust, through localized quenching of a melt. Note that this xenolith yields the lowest equilibration temperature of the suite (Table 1 and [20]), implying it was derived from a relatively shallow level. The zircons became closed to Pb loss by ca. 240 Ma ago.

5.4. 83-157 metapelite

Zircons in metapelitic xenolith 83-157 also fall into two morphological categories: (1) clear, rounded zircons, and (2) pale yellow, elongate zircons (Fig. 2H). The elongate zircons make up about one quarter of the zircon population. Inclusions are not abundant in either type of zircon, but elongate apatite is present in the elongate zircons and Fe-sulfide and rutile were observed in the round zircons.

The Th and U contents and Th/U ratios correlate with zircon morphology; the round zircons have low overall Th and U concentrations and high Th/U, whereas the elongate zircons have higher Th and U concentrations and lower Th/U (Fig. 3D).

Analyses of the round zircons are all within error of concordia at 250 ± 20 Ma. The elongate zircons fall into two age groups: (1) all but one define a chord between 1570^{+100}_{-115} Ma and 225^{+94}_{-77} Ma (model 3, MSWD = 2 [30]), and (2) one zircon (#2, Table 2) has a 2060 Ma concordant core, an interior zone showing ~ 50% Pb loss, probably at 240 Ma, and an outer rim which is nearly concordant at 1580 Ma (Fig. 4D). This zircon appears to be an inherited grain which crystallized at ~ 2060 Ma, was overgrown at 1580 and lost Pb at 240 Ma. Interestingly, none of these chronologically unique regions are optically distinguishable.

Several analyses from this sample (grains 3, 7, 16 and 20) plot above the concordia. This feature, which is rare in conventional zircon analyses, is occasionally seen in ion probe analyses because of the ability of the ion probe to detect very small scale variation in Pb/U and Pb/Th within crystals [31]. Reverse discordance is caused either by Pb gain relative to U and Th, or U and/or Th loss relative to Pb. In one of the zircons analyzed here (zircon 3) a correlation between Pb ppm and Pb/U and Pb/Th is observed, suggesting that Pb gain has occurred. The remaining analyses show no such correlation, but all have excesses of Pb relative to Th as well as to U, also suggesting Pb gain. The fact that all of the reversely discordant analyses fall along the discordance line defined by the normally discordant analyses shows that the movement of Pb (and possibly U and Th) within the zircons occurred at the time of the high-grade metamorphism.

Elongate zircons like the ones found in this sample may form either by crystallization from a magma or during regional metamorphism. Thus the age of the sediment is poorly constrained. If the elongate zircons crystallized from a melt, then

the sedimentary protolith of this xenolith must have formed after 1580 Ma, but prior to 250 Ma when it underwent high-grade metamorphism. Alternatively, if the elongate zircons are metamorphic, then the sediment age could be anywhere from > 1580 to nearly 250 Ma, if the source rock was confined to Proterozoic lithologies. In either case, the lack of zircon ages between 1580 and 240 Ma suggests that the sediment was not deeply buried before 250 Ma.

5.5. 85-100 metagabbro

Zircons in mafic xenolith 85-100 are round to elongate and clear. Many show parallel cleavage traces or partings. Inclusions are uncommon, but elongate apatite and rutile were observed.

Th and U concentrations as well as Th/U ratios are highly variable, but Th/U peaks at 1.1–1.2 (excluding the multiple analyses of grain 1) (Table 2, Fig. 3E). There is no correlation between Th/U and Th or U concentrations.

$^{206}Pb/^{238}U$ ages range from 250 Ma to 1140 Ma (Fig. 4E). The older zircons are elongate, but not all elongate zircons are old. There is no correlation between Th/U and age. Of the 13 zircons analyzed, 8 fall on, or near, concordia between 250 and 400 Ma, the other 5 fall within error of concordia and yield $^{206}Pb/^{238}U$ ages between 490 and 1140 Ma (Fig. 3E). The age of one 780 Ma zircon's rim (#10) is 370 Ma, suggesting either Pb loss or rim growth at this time.

The considerable age range for the zircons, coupled with their highly variable Th/U and Th and U concentrations suggests that these zircons are xenocrystic. This is consistent with the bulk rock chemistry of 85-100, which is similar to that of an oversaturated basaltic melt [20] in which zircon is not a stable phase for normal Zr concentrations [32]. The clustering of zircon ages between 400 and 250 Ma may represent metamorphic zircon growth, starting at 400 Ma, with either a Pb loss event at 250 Ma, or continuous Pb loss until 250 Ma.

5.6. 85-120 metagabbro

Zircons in mafic xenolith 85-120 are relatively scarce (three is only 63 ppm Zr in the whole rock, Table 1). These zircons are colorless and generally round. Cleavage traces occur in several zircons; mineral inclusions were not observed.

Th and U concentrations as well as Th/U ratios in these zircons are highly variable (for example U ranges from 20 to 1500 ppm, Table 2), with no obvious peak in Th/U (Fig. 3F). Many of these zircons have very low U abundances ($\leqslant 20$ ppm), which coupled with their relatively young age, make precise analyses very difficult to obtain (note several zircons with 1 ppm radiogenic Pb in Table 2). Several of these low-U zircons were analyzed in order to ensure that they do not represent a chronologically distinct population and the remainder were avoided. Therefore, the U contents listed in Table 2 are biased towards the higher values for the population.

$^{206}Pb/^{238}U$ ages range from 215 to 340 Ma and nearly all zircons are concordant (Fig. 4F). There is no correlation between Th/U and age.

The bulk composition of this xenolith is also similar to an oversaturated basaltic melt [20], therefore, these zircons are either xenocrystic or grew during metamorphism. If they are xenocrysts, the age of this rock may correspond to the age of Pb loss (ca. 250 Ma), which may have been caused by incorporation of the zircons into a basaltic magma. Alternatively, if the zircons grew as a metamorphic phase within the rock, the rock must have crystallized prior to 350 Ma with zircon growth beginning at 350 Ma, and Pb loss or continued zircon growth at or until 250 Ma.

5.7. 83-159 mafic restite

Zircons in mafic xenolith 83-159 are comparatively large (up to 300 μm) and clear, and many contain prominent cleavage traces, which are oriented parallel to the *c*-axis (Fig. 2L). Inclusions of acicular and tabular apatite, sulfides, pargasitic amphibole and melt (characterized by an ovoid shape and immobile, irregular vapor bubble, Fig. 2I) are present in the centers of some zircons. The melt inclusions are often associated with apatite crystals, suggesting the apatites may have acted as a trapping mechanism for the melts [27, Ch. 2]. Under high magnification (i.e., $\sim 800\times$) euhedral daughter crystals of amphibole and sulfide are visible within the melt inclusions, showing that partial to total recrystallization has occured (Fig. 2I, cf. [27]). Electron probe analyses of the daughter crystals and matrix material for several of these inclusions are given in Table 3. Reintegration of the melt inclusion compositions using probe

analyses and optical estimates of relative proportions yields an intermediate composition; this can be considered a very rough estimate of the melt composition from which the zircon crystalllized. CO_2-rich fluid inclusions were observed in two zircons. These fluid inclusions occur within planes that cross-cut crystal growth boundaries (Fig. 2J, K), implying they were trapped after initial crystallization.

The Th and U concentrations and Th/U ratios in these zircons are the most uniform in the suite (Table 2). Th/U ratios are all significantly less than 1.0, with a peak at 0.3 (Table 2; Fig. 3G). In contrast to this overall uniformity, Pb concentrations were observed to vary dramatically within single grains, even within a given analysis (as witnessed by the variable size of the ^{206}Pb peak on the chart recorder). Thus, Pb concentrations in these zircons are highly variable on a submicron scale.

$^{206}Pb/^{238}U$ ages range from 175 to 1590 Ma (excluding the reverse discordant analyses). Regression of the older zircon data ($^{206}Pb/^{238}U \geqslant 0.060$, $n = 20$) yields a chord with an upper intercept of 1520^{+150}_{-190} Ma and a lower intercept of 260^{+140}_{100} Ma (model 2, MSWD = 2.8 [30], Fig. 4G). The scatter of the younger zircons along concordia between 200 and ~ 350 Ma is similar to that observed in the previously described samples. It is likely that the cause of the scatter in the younger zircons (either slow cooling after a 350 Ma metamorphism or a second metamorphism at ~ 200 Ma) also contributed to the scatter in the data for the older zircons, resulting in a rather high MSWD for the regression. Th/U does not correlate with age, but multiple spot analyses within single crystals show a negative correlation between Th/U and $^{206}Pb/^{238}U$ age, suggesting that Pb loss was accompanied by preferential U loss during metamorphism. In several instances the ion beam intersected cleavage traces in the zircons (denoted with an § in Table 2). The analyses yield some of the youngest $^{206}Pb/^{238}U$ ages, suggesting that recent Pb loss may have occurred in the vicinity of these fractures.

The zircons in this sample originally crystallized around 1520 Ma ago in an intermediate to felsic melt. During the late Paleozoic this rock underwent high-grade metamorphism, accompanied by extraction of a partial melt leaving a mafic residue. This event was accompanied by severe Pb loss in the zircons. Recent Pb loss was facilitated by the presence of cleavage fractures, which may have formed as a result of decompression during rapid ascent of the xenolith in the pipe.

6. Discussion

6.1. Lower crustal history

The inclusion and geochronologic data presented above can be related to the regional geology to produce a model of how and when the lower crust formed. The major orogenic events within the Georgetown Inlier as delineated by Black et al. [16] and Black [17] through Rb-Sr geochronology are: (1) amphibolite facies metamorphism and granite intrusion at 1570 ± 20 Ma; (2) intrusion of granites in the southeastern Georgetown Inlier at 400 Ma, accompanied by retrogression in the eastern portion of the Georgetown metamorphics (from Rb-Sr biotite age); (3) eruption of extensive calc-alkaline felsic volcanics and intrusion of high-level granites between 320 and 270 Ma throughout the eastern Georgetown Inlier.

The ages derived from zircons in the xenoliths correlate well with these events. The 320 to 270 Ma granite- and felsic volcanic-forming orogeny was manifested in the lower crust by partial melting and regional high-grade metamorphism. Many of the xenoliths appear to have formed during this event, but several may have formed during the Proterozoic and have undergone granulite facies metamorphism at this time.

Four of the seven xenoliths appear to have formed during the late Paleozoic event. The two felsic xenoliths, 83-162 and 83-160, were formed by partial melting of the deep crust (some of which may have been Proterozoic, as evidenced by the one inherited zircon with an age of 2200 Ma) and did not move far from their sources. The mafic xenolith which is inferred to have formed as a cumulate from a felsic magma (85-107) also crystallized during this event. It is likely that all these samples formed and remained in the lower crust, as the preservation of unmetamorphosed 300 Ma felsic ash-flows near Hill 32 precludes substantial post-Paleozoic uplift. A second mafic xenolith with a basaltic melt composition (85-120) may represent a mantle-derived melt which

intruded the lower crust during this orogeny, thus suggesting a mantle heat source.

The mafic restite xenolith, 83-159, originally crystallized in the Proterozoic, but underwent high-grade metamorphism, which was accompanied by partial melt extraction in the late Paleozoic. The Proterozoic protolith for this mafic xenolith was an igneous rock of intermediate composition, as evidenced by the recrystallized melt inclusions in the cores of the zircons.

Similarly, metasedimentary xenolith 83-157 originally formed during the Proterozoic, but underwent high-pressure granulite facies metamorphism ~ 250 Ma ago. Because earlier metamorphic events are not recorded in the zircons, it seems likely that this age marks the time at which the rock was transported into the lower crust. The lack of significant erosion in this area since the late Paleozoic suggests that the mechanism responsible for bringing this supracrustal rock into the lower crust did not produce an isostatically unstable thickened crust.

Only one mafic xenolith, 85-100, potentially records the 400 Ma granite-forming event. This mafic xenolith contains xenocrystic zircons, but most zircons have ages between 400 and 250 Ma, suggesting that this rock, which has a basaltic composition, may have intruded the lower crust at 400 Ma and was later metamorphosed in the late Paleozoic.

6.2. Pb-loss patterns

All of the xenoliths investigated in this study record a late Paleozoic/early Mesozoic event and in all but one sample (83-157) the young zircons yield a range of concordant ages generally between 320 and 200 Ma. The 120 Ma spread in ages of the young zircons may have been produced in three possible ways. All entail either metamorphism or initial crystallization at ~ 320 Ma which was succeeded by one of the following: (1) a metamorphic event at 200 Ma which caused partial to complete Pb loss accompanied by new zircon growth. (2) slow cooling accompanied by diffusional Pb loss until 200 Ma, at which time the zircons passed below the Pb blocking temperature, or (3) recent Pb loss (i.e., ~ 0 Ma) due to either heating during entrainment of the xenolith in the basaltic host, exposure and weathering at the earth's surface or a relatively young thermal metamorphism. Of these possible causes of the spread in young zircon ages, slow cooling in the lower crust following the late Paleozoic orogeny ((2) above) seems the most plausible.

Recent Pb loss cannot explain the data for the following reasons. The length of time the xenoliths are carried by the basaltic magma (9–18 hours, calculated after Spera [33], from the fact that the host basalt also carries dense peridotite xenoliths) is too short to allow significant diffusion of Pb out of zircon, even if the xenoliths were heated to 1200 °C. Recent Pb loss in zircons caused by weathering is believed to be associated with structural damage due to the radioactive decay of U; damaged zones generally appear as darker, metamict regions within the zircons which are readily etched by HF acid [34]. None of the zircons examined here show deep coloration and attempts to etch heterogeneous zircons have failed (a polished mount was placed over hot concentrated HF for several minutes). These observations suggest that these zircons have little radiation-induced structural damage, possibly due to annealing at the high ambient temperatures in the lower crustal environment, and have therefore not suffered recent Pb loss. If the age spread is the result of recent Pb loss due to a young thermal metamorphism, it is peculiar that none of the zircons have lost more than 40% of their radiogenic Pb, so that none fall below about 200 Ma on the concordia diagram. An example of the Pb-loss behavior of zircons due to thermal metamorphism is provided by the two Proterozoic samples which underwent high grade metamorphism in the late Paleozoic (83-157 and 83-159). In these samples, the metamorphism caused variable degrees of Pb loss so that the zircons plot along the length of a chord between their Proterozoic age (~ 1570 Ma) and their metamorphic age (~ 250 Ma). Similar Pb-loss patterns would be expected if the zircons underwent a young ($\leqslant$ 100 Ma) thermal metamorphism, yet only $\leqslant$ 40% Pb loss is observed.

It also seems unlikely that the age spread can be attributed to a second metamorphic event at 200 Ma ((1) above) since there is no surface manifestation of it, such as igneous activity or tectonic uplift and erosion. Therefore, the 120 Ma spread in age for the young zircons is attributed to slow cooling in a lower crustal environment following the 320 Ma event. Such a cooling time

scale is entirely consistent with that predicted for magmatically heated orogenic belts which have undergone little erosion [35].

6.3. The nature of the late Paleozoic orogeny

Inferences about the nature of the late Paleozoic orogeny can be gleaned from the above geochronologic data. Firstly, it is obvious that intense heating of the lower crust occurred during the late Paleozoic event. The source of the heat is most likely mantle-derived basaltic melts, such as represented by two-pyroxene granulite 85-120, and possibly other zircon-free mafic xenoliths such as those described by Rudnick and Taylor [20]. The intense thermal input resulted in crustal melting and the formation of felsic rocks, some of which remained at deep levels (83-160 and 83-162) while others rose to high levels in the crust. Secondly, little uplift accompanied the late Paleozoic orogeny, since late Paleozoic felsic ash-flows are well preserved at the surface, and the xenoliths exhibit neither textures nor mineral reactions indicative of uplift (Table 1 and [20]). Despite the lack of significant uplift, at least some thrusting occurred during the orogeny since a demonstrably supracrustal rock (metasediment 83-157) was apparently brought to granulite facies conditions at this time. This coincides with the timing of the movement along the Palmerville fault zone [15].

The above features are consistent with a continental arc setting, where basalts are produced above a subducting slab and intruded into the continental crust, causing high-grade metamorphism and partial melting [35]. Such a setting has been suggested for the late Paleozoic of north Queensland based upon the chemistry of the eruptive rocks and regional structures [18,19].

7. Conclusions

The major conclusions from this study are as follows:

(1) Ion probe analyses of zircons from xenoliths can provide tight constraints on crystallization and metamorphic ages of these rocks, where other isotopic systems, for a variety of reasons, fail to do so.

(2) Mineral, fluid and melt inclusions within zircons provide important information on the origin of the zircon and the petrogenesis of the host rock. In particular, felsic to intermediate melt inclusions in zircons from mafic rocks necessitate a two-stage history for these samples.

(3) The U-Pb zircon ages for the McBride province lower crustal xenoliths correlate well with the surface geological history, illustrating that lower crustal formation and modification is often manifested at the earth's surface.

(4) All of the xenoliths record a major tectonothermal event about 300 Ma ago which was accompanied by partial melting, crystal fractionation and granulite facies metamorphism of all the rocks. The zircons in these rocks then experienced variable degrees of Pb loss for a well-defined period of about 100 Ma as they cooled in the deep crust.

(5) The late Paleozoic metamorphic ages, coupled with the absence of appreciable erosion since that time, proves that the xenoliths are not fragments of high-grade rocks which were picked up by the basalt near the earth's surface.

(6) Several xenoliths record Proterozoic ages illustrating the antiquity of at least part of the lower crust in this region.

Acknowledgements

We are indebted to Bill Compston for making available valuable time on SHRIMP and for sharing his expertise in data reduction methods. We also thank Nick Ware for assistance with electron probe analyses and Trevor Ireland and John Foster for assistance with ion probe analyses. Ben Harte, Heinz-Gunter Stosch, Joe Stolz, Martin Dodson, Ed Roedder and Chris Hawkesworth provided helpful comments. Peter Zeitler kindly provided us with PLONC.

Appendix A—Correction for scattered ions, first analytical session

Analyses of young zircons performed when SHRIMP was operating at high background levels were found to have overestimated the $^{207}Pb/^{206}Pb$ ratio. When repeat analyses of these same spots were performed when SHRIMP was operating at low background levels, the zircons were shown to be concordant. The overestimation of $^{207}Pb/^{206}Pb$ was directly related to underestimation of the background counts at mass 207 and is proportional to the overall beam intensity.

Analyses obtained during high-background operating conditions were corrected in the following manner: for zircons with nearly the same $^{206}Pb/^{238}U$ age, a positive, linear correla-

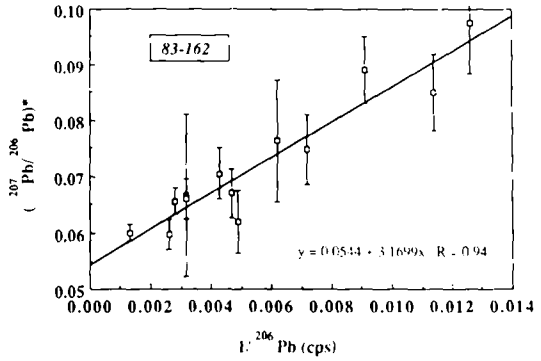

Fig. A-1. Inverse of ^{206}Pb counts/s versus the radiogenic $^{207}Pb/^{206}Pb$ ratio for zircons from 83-162. Error bars represent 1σ standard deviation. The slope is equal to the excess counts per second at the ^{207}Pb mass.

tion exists between the radiogenic $^{207}Pb/^{206}Pb$ ratio and the reciprocal of radiogenic ^{206}Pb counts/second (a measure of the amount of total radiogenic Pb in the sample), i.e. the lower the Pb content, the larger the apparent age of the zircon (Fig. A-1). Such a relationship reflects the addition of a constant count ratio (C) to the Pb peaks. As ^{207}Pb is the smallest of the Pb peaks in these young zircons, it is the only peak significantly affected by this constant. The slope of the line in Fig. A-1 is equal to C, which is in units of counts/second; the intercept is equal to the true $^{207}Pb/^{206}Pb$ ratio of the zircons (around 0.054). The constant can then be subtracted from the ^{207}Pb counts/second to obtain the corrected ^{207}Pb count rate. C varies from sample to sample depending upon beam intensity; the higher the beam intensity (as reflected in the counts of Zr_2O), the higher C becomes. By dividing C by the average Zr_2O counts/second for each analytical session, the effects of beam intensity are overcome (C'). For samples where all the young zircons are expected to be concordant (83-162 and 85-120), C can be determined directly ($C' = 2.6 \times 10^{-4}$ for 83-162; $C' = 1.7 \times 10^{-4}$ for 85-120). For samples in which some of the zircons are expected to be discordant (i.e., 83-159) an average value of C' as determined for other samples was used. All analyses performed during high background conditions were corrected in this manner, however, the correction only significantly affects the youngest zircons which have the lowest ^{207}Pb counts. All corrected samples are designated with italicized numbers in Table 2.

References

1 R.L. Rudnick, W.F. McDonough, M.T. McCulloch and S.R. Taylor, Lower crustal xenoliths from Queensland, Australia: evidence for deep crustal assimilation and fractionation of continental basalts. Geochim. Cosmochim. Acta 50, 1099–1115, 1986.

2 H.-G. Stosch and G.W. Lugmair, Evolution of the lower continental crust: granulite facies xenoliths from the Eifel, West Germany, Nature 311, 368–370, 1984.

3 B. Harte, P.M. Jackson and R.M. Macintyre, Age of mineral equilibria in granulite facies nodules from kimberlites, Nature 291, 147–291, 1981.

4 S.H. Richardson, E.R. Padovani and S.R. Hart, The gneiss syndrome: Nd- and Sr-isotopic relationships in lower crustal xenoliths, Kilbourne Hole, New Mexico, EOS 61, 388, 1980.

5 O. Van Breemen and C.J. Hawkesworth, Sm-Nd isotopic study of garnets and their metamorphic host rocks, Trans. R. Soc. Edinburgh 71, 97–102, 1980.

6 S.M. Kay and R.W. Kay, Thermal history of the deep crust inferred from granulite xenoliths, Queensland, Australia, Am. J. Sci. 283-A, 486–513, 1983.

7 R.L. Rudnick and S.R. Taylor, Petrology and geochemistry of lower crustal xenoliths from northern Queensland and inferences on lower crustal composition, Spec. Publ. Geol. Soc. Aust., in press, 1987.

8 G.L. Davis and E.S. Grew, Age of zircon from a crustal xenolith, Kilbourne Hole, New Mexico, Carnegie Inst. Washington Yearb. 77, 897–898, 1977.

9 A.N. Halliday, M. Aftalion, B.G.J. Upton, P. Aspen and J. Jocelyn, U-Pb isotopic ages from a granulite facies xenolith from Partan Craig in the Midland valley of Scotland, Trans. R. Soc. Edinburgh 75, 71–74, 1984.

10 R.W. Kay and S.M. Kay, The nature of the lower crust: inferences from geophysics, surface geology, and crustal xenoliths, Rev. Geophys. Space Phys. 19, 271–297, 1980.

11 W.L. Griffin and S.Y. O'Reilly, The lower crust in eastern Australia: xenolith evidence, in: The Nature of the Lower Continental Crust, B.J. Dawson, J. Hall and K.H. Wedepohl, eds., Geol. Soc. London Spec. Publ. 24, 363–374, 1986.

12 L.P. Black, I.S. Williams and W. Compston, Four zircon ages from one rock: the history of a 3930 Ma-old granulite from Mount Sones, Enderby Land, Antarctica, Contrib. Mineral. Petrol. 94, 427–437, 1986.

13 P.J. Stephenson and T.J. Griffin, Cainozoic volcanicity in north Queensland, Excursion Guide No. 7A, 25th Int. Geol. Congr., 39 pp., 1976.

14 D.A. White, Geology of the Georgetown-Clark River area, Queensland, Bur. Mineral. Res. Aust. Bull. 71, 165 pp., 1965.

15 R.D. Shaw, J.F. Fawckner and R.J. Bultitude, The Palmerville fault system: a major imbricate thrust system in the Northern Tasmanides, North Queensland, Aust. J. Earth Sci. 34, 69–93, 1987.

16 L.P. Black, T.H. Bell, M.J. Rubenach and I.W. Withnall, Geochronology of discrete structural-metamorphic events in a multiply deformed Precambrian terrain, Tectonophysics 54, 103–137, 1979.

17 L.P. Black, Rb-Sr systematics of the Claret Creek ring complex and their bearing on the origin of Upper Palaeozoic igneous rocks in northeast Queensland, J. Geol. Soc. Aust. 27, 157–166, 1980.

18 J.W. Sheraton and B. Labbone, Petrology and geochemistry of acid igneous rocks of northeast Queensland, Bur. Mineral Res. Bull. 169, 139 pp., 1978.

19 B.S. Oversby, L.P. Black and J.W. Sheraton, Late Palaeozoic continental volcanism in northeastern Queensland, in: The Geology and Geophysics of Northeastern Australia,

R.A. Henderson and P.J. Stephenson, eds., pp. 247–268, Geological Society Australia, Queensland Division, 1980.
20 R.L. Rudnick and S.R. Taylor, The composition and petrogenesis of the lower crust: a xenolith study, J. Geophys. Res., in press, 1987.
21 W. Compston, I.S. Williams and C. Meyer, U-Pb geochronology of zircons from lunar breccia 73217 using a sensitive high mass-resolution ion microprobe, Proc. 14th Lunar Planet. Sci. Conf., Part 2, J. Geophys. Res. 89, B525–B534, 1984.
22 W. Compston, P.D. Kinny, I.S. Williams and J.J. Foster, The age and Pb loss behaviour of zircons from the Isua supracrustal belt as determined by ion microprobe, Earth Planet. Sci. Lett. 80, 71–81, 1986.
23 F. Tera and G.J. Wasserburg, U-Th-Pb systematics in three Apollo 14 basalts and the problem of initial Pb in lunar rocks, Earth Planet. Sci. Lett. 14, 281–304, 1972.
24 R.H. Steiger and E. Jäger, Subcommission on Geochronology: Convention on the use of decay constants in geo- and cosmo-chronology, Earth Planet. Sci. Lett., 36, 359–362, 1977.
25 P. Kresten, P. Fels and G. Berggren, Kimberlitic zircons—a possible aid in prospecting, Miner. Deposita 10, 47–56, 1975.
26 J. Touret, Fluid inclusions in high grade metamorphic rocks, in: Short Course in Fluid Inclusions: Applications to Petrology, L.S. Hollister and M.L. Crawford, eds., Mineral. Assoc. Can. Short Course Handb. 6, 182–208, 1981.
27 E. Roedder, Fluid Inclusions, P.H. Ribbe, ed., Rev. Mineral. 12, 644 pp., 1984.
28 L.H. Ahrens, Some observations on the uranium and thorium distribution in accessory zircon from granitic rocks, Geochim. Cosmochim. Acta 29, 711–716, 1965.
29 P.J. Wyllie, K.G. Cox and G.M. Biggar, The habit of apatite in synthetic systems and igneous rocks, J. Petrol. 3, 238–243, 1962.
30 G.A. McIntyre, C. Brooks, W. Compston and A. Turek, The statistical assessment of Rb-Sr isochrons, J. Geophys. Res. 71, 5459–5468, 1966.
31 I.S. Williams, W. Compston, L.P. Black, T.R. Ireland and J.J. Foster, Unsupported radiogenic Pb in zircon: a cause of anomalously high Pb–Pb, U-Pb and Th-Pb ages, Contrib. Mineral. Petrol. 88, 322–327, 1984.
32 J.E. Dickinson, Jr. and P.C. Hess, Zircon saturation in lunar basalts and granites, Earth Planet. Sci. Lett. 57, 336–344, 1982.
33 F.J. Spera, Aspects of magma transport, in: Physics of Magmatic Processes, R.B. Hargraves, ed., pp. 265–323, Princeton University Press, 1980.
34 T.E. Krogh and G.L. Davis, Alteration in zircons and differential dissolution of altered and metamict zircon, Carnegie Inst. Washington Yearb. 74, 619–623, 1974.
35 P.R.A. Wells, Thermal models for the magmatic accretion and subsequent metamorphism of continental crust, Earth Planet. Sci. Lett. 46, 253–265, 1979.
36 P.R.A. Wells, Pyroxene thermometry in simple and complex systems, Contrib. Mineral. Petrol. 62, 129–139, 1977.
37 D.J. Ellis and D.H. Green, An experimental study of the effect of Ca upon garnet-clinopyroxene Fe-Mg exchange equilibria, Contrib. Mineral. Petrol. 71, 13–22, 1979.
38 D. Perkins, III and R.C. Newton, Charnockite geobarometers based on coexisting garnet-pyroxene-plagioclase-quartz, Nature 299, 409–413, 1981.
39 J.M. Ferry and F.S. Spear, Experimental calibration of the partitioning of Fe and Mg between biotite and garnet, Contrib. Mineral. Petrol. 66, 113–117, 1978.